Materials Advances

ROYAL SOCIETY OF CHEMISTRY

PAPER

View Article Online
View Journal | View Issue

Open Access Article. Published on 13 May 2022. Downloaded on 10/20/2025 10:18:24 PM.
This article is licensed under a Creative Commons Attribution-NonCommercial 3.0 Unported Licence.

Check for updates

Cite this: *Mater. Adv.*, 2022, 3, 4724

Molecular conductors from bis(ethylenedithio)tetrathiafulvalene with tris(oxalato)gallate and tris(oxalato)iridate†

Toby J. Blundell,[a] Alexander L. Morritt,[a] Elizabeth K. Rusbridge,[a] Luke Quibell,[a] Jakob Oakes,[a] Hiroki Akutsu,[b] Yasuhiro Nakazawa,[b] Shusaku Imajo,[c] Tomofumi Kadoya,[d] Jun-ichi Yamada,[d] Simon J. Coles,[e] Jeppe Christensen[e] and Lee Martin *[a]

Received 5th April 2022,
Accepted 25th April 2022

DOI: 10.1039/d2ma00384h

rsc.li/materials-advances

We present the synthesis, crystal structures and conducting properties of six new BEDT-TTF radical-cation salts with the tris(oxalato)gallate or -iridate anion. The use of halobenzenes gives 4 : 1 β″ metallic or superconducting salts with tris(oxalato)gallate – fluorobenzene (PhF) or chlorobenzene (PhCl) as a guest molecule gives a metal, whilst the larger bromobenzene (PhBr) or iodobenzene (PhI) gives a superconductor. A 4 : 1 pseudo-κ semiconducting salt is obtained with benzonitrile as the guest molecule for tris(oxalato)iridate, and a novel 5 : 1 metal–insulator phase with tris(oxalato)iridate is also reported.

Introduction

The organic donor molecule BEDT-TTF has produced the largest number of molecular superconductors, with the highest superconducting T_c being 11.6 K at ambient pressure in κ-(BEDT-TTF)$_2$Cu[N(CN)$_2$]Br,[1] and 14.2 K under pressure in β′-(BEDT-TTF)$_2$ICl$_2$.[2]

Multifunctionality has been achieved in BEDT-TTF salts with the use of various transition-metal complexes with particular focus on the tris(oxalato)metallate anion to combine conductivity in the same lattice with paramagnetism,[3] anti-ferromagnetism,[4] ferromagnetism,[5] proton conductivity,[6] or chirality.[7] The first radical-cation salt in this family, β″-(BEDT-TTF)$_4$[(A)Fe(C$_2$O$_4$)$_3$]·PhCN[3] (PhCN = benzonitrile, A = initially reported as H_2O and later as H_3O^+), was synthesised by the group of Professor Peter Day at The Royal Institution of Great Britain in 1995.[3] This salt has a superconducting T_c of 8.5 K which is still the highest superconducting T_c for the BEDT-TTF-tris(oxalato)metallate salts to date.[8] A polymorph, pseudo-κ-(BEDT-TTF)$_4$[(A)Fe(C$_2$O$_4$)$_3$]·PhCN (A = K^+ and NH_4^+),[3] differing only in the spatial arrangement of the enantiomers of Fe(C$_2$O$_4$)$_3$, was also reported. This initial discovery opened pathways to produce a family of materials which now numbers well over a hundred examples with the majority of the structures being 4 : 1 salts of the β″ or pseudo-κ type.[8]

The packing of the BEDT-TTF donor layers determines the conducting behaviour and this packing can be subtly changed through modifications of the neighbouring anion layers. The anion layers form a hexagonal network of tris(oxalato)metallate with a counter cation which produces honeycomb cavities capable of accommodating a guest molecule of the solvent used for electrocrystallisation. Changing the metal ion of Fe(C$_2$O$_4$)$_3^{3-}$ from iron (Al^{3+},[9] Co^{3+},[9] Cr^{3+},[10] Ga^{3+},[11] Mn^{3+},[12] Rh^{3+},[13] or Ru^{3+} [9,14]) or changing the counter cation (A = H_3O^+, K^+, NH_4^+)[3] has a small effect on the donor packing arrangement. However, changing the size and shape of the included solvent guest molecule can have a marked effect on the donor packing and thus the conducting properties.

Guest molecules similar in size to benzonitrile produce isostructural 4 : 1 β″ salts, whilst bulkier guest molecules protrude on one side of the anion layer to produce two different faces for the anion layer which leads to a different BEDT-TTF packing type on either side of the anion layer (*e.g.* α + β″ with PhCH$_2$CN[15] or PhCH(OH)CH$_3$,[7] or α + pseudo-κ with 1,2-Br$_2$Ph[16]). With smaller guest molecules (CH$_3$NO$_2$, CH$_3$CN, and CH$_2$Cl$_2$)[17] a 3 : 1 semiconducting salt is obtained. In some salts 18-crown-6 ether, which is added to aid solubility of the

[a] School of Science and Technology, Nottingham Trent University, Clifton Lane, Clifton, Nottingham, NG11 8NS, UK. E-mail: lee.martin@ntu.ac.uk
[b] Department of Chemistry, Graduate School of Science, Osaka University, 1-1 Machikaneyama-cho, Toyonaka, Osaka 560-0043, Japan
[c] The Institute for Solid State Physics, The University of Tokyo, Kashiwa, Chiba 277-8581, Japan
[d] Graduate School of Material Science, University of Hyogo, Kamigori-cho, Ako-gun, Hyogo, 678-1297, Japan
[e] School of Chemistry, Faculty of Natural and Environmental Sciences, University of Southampton, Highfield, Southampton, SO17 1BJ, UK

† CCDC 2163082–2163089 contains supplementary X-ray crystallographic data for **1–6**, respectively. For crystallographic data in CIF or other electronic format see DOI: https://doi.org/10.1039/d2ma00384h

© 2022 The Author(s). Published by the Royal Society of Chemistry

Open Access Article. Published on 13 May 2022. Downloaded on 10/20/2025 10:18:24 PM.
This article is licensed under a Creative Commons Attribution-NonCommercial 3.0 Unported Licence.

ammonium or potassium salt of the anion, is included in the lattice to produce a 2:1 superconducting salt, β″-(BEDT-TTF)$_2$[(H$_2$O)(NH$_4$)$_2$M(C$_2$O$_4$)$_3$]·18-crown-6 (M = Cr^{3+} or Rh^{3+})[18] or a 2:1 proton conductor/metal β″-(BEDT-TTF)$_4$[(A)M(C$_2$O$_4$)$_3$]$_2$·[(A)^{2}18-crown-6](H$_2$O)$_5$ (M = Cr^{3+} or Ga^{3+}, A = H_3O^+ or NH_4^+).[6]

A variety of other unusual donor and anion packings have also been obtained with $Fe(C_2O_4)_3^{3-}$,[19] as is also the case when replacing the M^{3+} ion with M^{4+} with dianionic $Ge(C_2O_4)_3^{2-}$.[20]

This paper reports the syntheses, structures and properties of six new additions to this family of BEDT-TTF salts with tris(oxalato)metallates of gallium and iridium. Four tris(oxalato)-gallate salts are 4:1 salts β″-(BEDT-TTF)$_4$[(H$_3$O)Ga(C$_2$O$_4$)$_3$]·halobenzene – fluorobenzene (PhF) or chlorobenzene (PhCl) as a guest molecule gives a metal, whilst the larger bromobenzene (PhBr) or iodobenzene (PhI) gives a superconductor. A semiconducting 4:1 salt pseudo-κ-(BEDT-TTF)$_4$[(H$_3$O)Ir(C$_2$O$_4$)$_3$]·benzonitrile (PhCN) is reported. The synthesis, structure and band calculations of a new 5:1 metal–insulator phase, β″-(BEDT-TTF)$_5$Ir(C$_2$O$_4$)$_3$·ethanol, are also reported.

Results and discussion

4:1 β″ salts with tris(oxalato)gallate

Isostructural salts **1–4** are new additions to the β″ family of BEDT-TTF radical-cation salts with the tris(oxalato)gallate anion. All four salts have the formula β″-(BEDT-TTF)$_4$[(H$_3$O)Ga(C$_2$O$_4$)$_3$]·guest (guest = PhF fluorobenzene **1**, PhCl chlorobenzene **2**, PhBr bromobenzene **3**, and PhI iodobenzene **4**). Salts **1–4** all crystallise in the monoclinic space group *C*2/*c* with an asymmetric unit consisting of two crystallographically independent BEDT-TTF molecules, half a $Ga(C_2O_4)_3^{3-}$ anion, half a H_3O^+ counter cation, and half a guest molecule.

Fig. 1 shows the layered structure of these salts which consists of alternating donor layers of BEDT-TTF and anion layers of $M(C_2O_4)_3^{3-}$/guest/H_3O^+. The two crystallographically independent BEDT-TTF molecules adopt a β″ packing motif in stacks along the *a*/*b* crystallographic axis (Fig. 2). The two independent BEDT-TTF molecules follow an AABBAA sequence within each stack. There are a number of side-to-side S···S interactions between donor stacks which are below the sum of the van der Waals radii (Table 1). Using the method of Guionneau *et al.*[21] to estimate the charge on a BEDT-TTF molecule from its C–S and C=C bond lengths we estimate charges of approximately +0.5 for all BEDT-TTFs (Table 2) as expected for

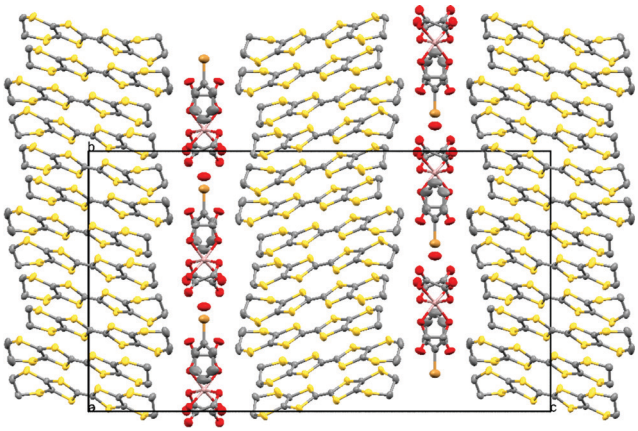

Fig. 1 Structure of **4** viewed down the *a* axis. Salts **1–4** are isostructural. Hydrogen atoms and minor disorder components are omitted for clarity.

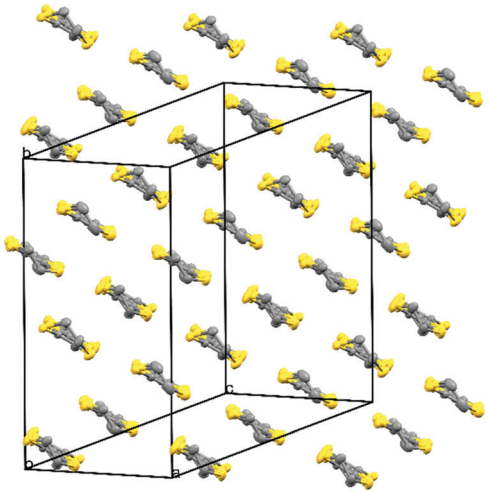

Fig. 2 Packing arrangement of the donor layer for **4**. Salts **1–4** are isostructural. Hydrogen atoms and minor disorder components are omitted for clarity.

Table 1 Short range interactions (>sum VdW radii) for donor cations in salts **1–4**

Contact (Å)	Ga-PhF (**1**)	Ga-PhCl (**2**)	Ga-PhBr (**3**)	Ga-PhI (**4**)
S1···S7	3.3817(19)	3.417(2)	3.4206(10)	3.4381(10)
S3···S7	3.5225(18)	3.517(2)	3.5041(10)	3.4915(10)
S2···S9	3.3397(19)	3.329(2)	3.3147(10)	3.297(4)
S2···S11	3.3811(18)	3.3792(19)	3.3695(10)	3.368(4)
S6···S15	3.528(2)	3.533(2)	3.5180(10)	3.5123(10)
S8···S15	3.612(2)	3.594(2)	3.5612(11)	3.5404(12)
S8···S10	3.600(2)	3.600(2)	3.5793(11)	3.5753(11)

Table 2 Average bond lengths (Å) in BEDT-TTF molecules in salts **1–4** with approximation of the charge on the molecules. $\delta = (b + c) - (a + d)$, $Q = 6.347 - 7.463\delta$[21]

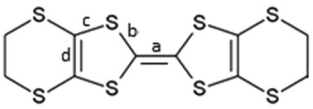

Salt	Donor	*a*	*b*	*C*	*D*	*δ*	*Q*
Ga-PhF	A	1.355	1.73725	1.7455	1.347	0.781	+0.52
1	B	1.360	1.73525	1.746	1.3475	0.774	+0.57
Ga-PhCl	A	1.360	1.744	1.747	1.3505	0.781	+0.52
2	B	1.357	1.741	1.745	1.352	0.777	+0.54
Ga-PhBr	A	1.358	1.738	1.748	1.346	0.782	+0.51
3	B	1.370	1.735	1.749	1.341	0.773	+0.58
Ga-PhI	A	1.360	1.7345	1.7425	1.3455	0.772	+0.59
4	B	1.359	1.73525	1.744	1.346	0.774	+0.57

Open Access Article. Published on 13 May 2022. Downloaded on 10/20/2025 10:18:24 PM.
This article is licensed under a Creative Commons Attribution-NonCommercial 3.0 Unported Licence.

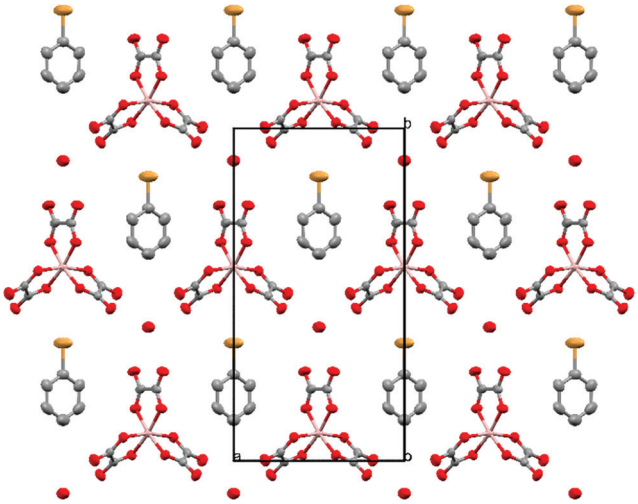

Fig. 3 Packing arrangement of the anion layer for **4**. Salts **1–4** are isostructural. Hydrogen atoms and minor disorder components are omitted for clarity.

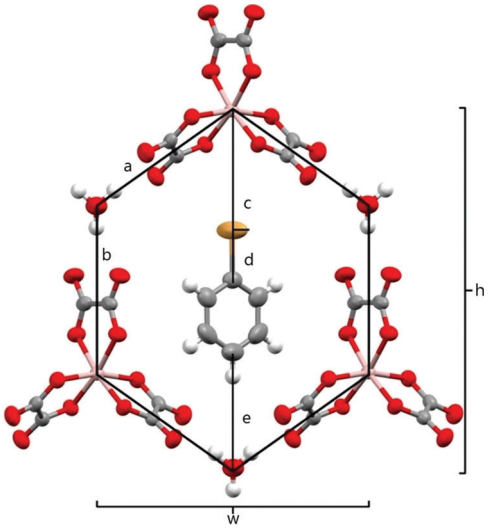

Fig. 4 Honeycomb cavity in the anion layer for **4** with measurement parameters labelled. Salts **1–4** are isostructural.

these 4 : 1 β″ salts where the anion layer has a 2-charge $[(H_3O)Ga(C_2O_4)_3]^{2-}$.

The anion layer is a honeycomb created using $M(C_2O_4)_3^{3-}$ anions and H_3O^+ cations with a guest solvent molecule in the hexagonal cavities (Fig. 3). Each anion layer consists of a single $M(C_2O_4)_3^{3-}$ enantiomer with adjacent layers being the opposite enantiomer to give a repeating ΔΛΔΛΔΛ pattern and a racemic lattice. The dimensions of the hexagonal cavities for salts **1–4** are defined in Fig. 4 and the values given in Table 3. It has previously been observed for rhodium[13] and iron[22] salts that increasing the size of the guest molecule from fluorobenzene to chlorobenzene to bromobenzene leads to an increase in the height and a decrease in the width of the cavity. In gallium salts we observe the same trend going from fluorobenzene to bromobenzene to iodobenzene, however the chlorobenzene salt has a longer height than bromobenzene and a narrower width than fluorobenzene.

The size, shape and orientation of the guest solvent molecule within the hexagonal cavity influence the order–disorder of the terminal ethylene groups of adjacent BEDT-TTF molecules which affects the transport properties or destabilises the superconducting transition.[8] The BEDT-TTF molecules in all of the salts **1–4** contain disordered ethylene groups (C1, C2, C9, and C10) irrespective of the guest solvent molecule present. In the case of **1** (Ga PhF) we also observe disorder in the position of fluoride on the guest molecule (Fig. 5). The fluoride occupies both the standard position, pointing directly at the metal atom along the *c* axis, as well as a roughly 16% occupancy at each *meta* position to the standard position. This results in a disordered component where the fluoride protrudes out of the cavity. Presumably, this is possible due to the small size of fluoride compared to the other substituents on the phenyl of the guest molecules, allowing this orientation to be favourable without interrupting the crystal packing.

The only previously reported β″ superconducting salts with the tris(oxalato)gallate anion incorporated the guest molecules pyridine (T_c = 1.5 K) or nitrobenzene (T_c = 7.5 K).[11] Guest molecules 2-chloropyridine or 2-bromopyridine show metallic behaviour down to 0.5 K.[23]

Table 3 Dimensions of the hexagonal cavity for salts **1–4** as shown in Fig. 4 and for salt **5** in Fig. 10 (*a*, *b*, *c*, *d*, *e*, *h* and *w*). δ is the angle of the plane of the halobenzene ring relative to the plane of the hexagonal cavity (measured as the least squares plane of the three gallium atoms)

Salt temp.	Ga-PhF (**1**) 294 K	Ga-PhCl (**2**) 293 K	Ga-PhBr (**3**) 293 K	Ga-PhI (**4**) 294 K	Ga-PhCN (**5**) 293 K
Distances (Å)					
a	6.259(4)	6.282(4)	6.279(2)	6.298(2)	6.288(4)
b	6.378(7)	6.395(7)	6.360(4)	6.349(4)	6.254(7)
c	4.802(14)	4.614(3)	4.5533(7)	4.5571(6)	*c* + *d* = 5.168(9)
d	1.311(18)	1.740(9)	1.889(5)	2.078(4)	0.950
e	4.674(17)	4.497(14)	4.405(7)	4.294(7)	5.375(14)
h	13.520(7)	13.597(7)	13.579(4)	13.658(4)	13.352(7)
w	10.2801(4)	10.2964(7)	10.2760(2)	10.2593(2)	10.38141(15)
O4-cation	2.960(6)	3.005(6)	3.022(4)	3.073(3)	2.930(7)
O6-cation	2.866(5)	2.851 (5)	2.839(3)	2.828(3)	2.899(5)
O1-cation	3.011(8)	3.013(8)	2.994(4)	2.986(4)	2.881(8)
Angles (°)					
δ	33.4(3)	32.7(2)	33.5(2)	34.60(16)	25.4(2)

 © 2022 The Author(s). Published by the Royal Society of Chemistry

Open Access Article. Published on 13 May 2022. Downloaded on 10/20/2025 10:18:24 PM.
This article is licensed under a Creative Commons Attribution-NonCommercial 3.0 Unported Licence.

A salt synthesised from potassium tris(oxalato)gallate with bromobenzene has previously been reported (β″-(BEDT-TTF)$_4$[$K_{0.33}(H_3O)_{0.67}Ga(C_2O_4)_3$]·PhBr)[11] and showed no superconductivity down to 0.5 K. Salt **3** is the isostructural salt starting from ammonium tris(oxalato)gallate with bromobenzene and shows superconductivity with a T_c of 3.0 K. When using ammonium tris(oxalato)gallate instead of potassium only the H_3O^+ counter cation is included in the lattice (β″-(BEDT-TTF)$_4$[$(H_3O)Ga(C_2O_4)_3$]·bromobenzene). The non-superconducting salt with $K_{0.33}(H_3O)_{0.67}$ has a *b* axis of 19.860(2) Å whilst the H_3O^+ salt (**3**) has a longer *b* of 19.9923(14) Å (both at 293 K).

Analysis of the crystal structures of the β″-(BEDT-TTF)$_4$[(A)M$(C_2O_4)_3$]·solvent salts by Imajo *et al.*[24] has revealed a correlation between the cell parameters and the conducting properties. Changing the size and shape of the included guest molecule has a marked effect on the cell parameters, especially the length of the *b* axis, with which the superconducting T_c can be correlated. The halogen atom of the guest molecule is directed along the *b* axis in these salts so we expect an increase of the *b* axis as the guest molecule is increased in size from PhF up to PhI. In these Ga salts the *b* axis for the PhCl salt **2** is longer than that of the PhBr salt **3** (Table 4‡). Salts **1** and **2** with smaller PhF and PhCl, respectively, do not show superconductivity (Fig. 6). Salts **3** and **4** with larger PhBr and PhI show superconducting T_cs of 3.0 K and 2.4 K respectively.

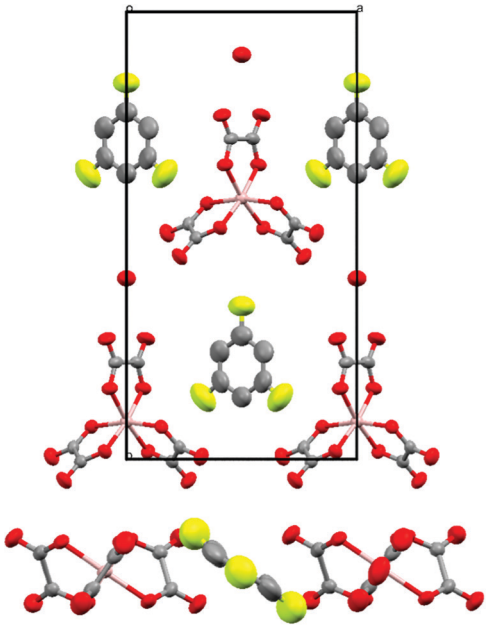

Fig. 5 Hexagonal cavity of **1** containing fluorobenzene showing the orientation of the disordered fluorine atoms. The major component (~68%) points directly at the gallium atom whereas the minor component (~16% each side) protrudes out of the cavity. Hydrogen atoms and minor disorder components are omitted for clarity.

‡ Crystal data **1**: $C_{52}H_{40}O_{13}S_{32}F_1Ga_1$, M = 1987.52, black block, a = 10.2801(4), b = 19.8975(10), c = 35.2455(13) Å, β = 92.680(3)°, U = 7201.5(5) Å^3, T = 294(2) K, space group $C2/c$, Z = 4, μ = 1.373 mm^{-1}, reflections collected = 19 058, independent reflections = 6022, R_1 = 0.0725, wR_2 = 0.1454 [$F^2 > 2\sigma(F^2)$], R_1 = 0.0891, wR_2 = 0.1542 (all data). Crystal data **2**: $C_{52}H_{40}O_{13}S_{32}Cl_1Ga_1$, M = 2003.93, black block, a = 10.2964(7), b = 19.9923(14), c = 35.423(3) Å, β = 93.080(3)°, U = 7281.3(9) Å^3, T = 293(2) K, space group $C2/c$, Z = 4, μ = 1.392 mm^{-1}, reflections collected = 21 117, independent reflections = 9327, R_1 = 0.0745, wR_2 = 0.1117 [$F^2 > 2\sigma(F^2)$], R_1 = 0.1483, wR_2 = 0.1447 (all data). Crystal data **3**: $C_{52}H_{40}O_{13}S_{32}Br_1Ga_1$, M = 2048.39, black block, a = 10.2880(3), b = 19.9599(6), c = 35.5191(8) Å, β = 93.392(2)°, U = 7280.98(16) Å^3, T = 293(2) K, space group $C2/c$, Z = 4, μ = 1.901 mm^{-1}, reflections collected = 39 889, independent reflections = 8997, R_1 = 0.0425, wR_2 = 0.0992 [$F^2 > 2\sigma(F^2)$], R_1 = 0.0537, wR_2 = 0.1057 (all data). Crystal data **4**: $C_{52}H_{40}O_{13}S_{32}I_1Ga_1$, M = 2095.38, black block, a = 10.2593(2), b = 20.0074(4), c = 35.5849(7) Å, β = 93.7398(18)°, U = 7288.7(2) Å^3, T = 294(2) K, space group $C2/c$, Z = 4, μ = 1.778 mm^{-1}, reflections collected = 35 658, independent reflections = 7838, R_1 = 0.0347, wR_2 = 0.0801 [$F^2 > 2\sigma(F^2)$], R_1 = 0.0385, wR_2 = 0.0819 (all data). Crystal data **5**: $C_{53}H_{39}O_{13}S_{32}N_1Ir_1$, M = 2115.99, black block, a = 10.38140(14), b = 19.6057(3), c = 35.5790(5) Å, U = 7241.56(18) Å^3, T = 150.00(10) K, space group $Pbcn$, Z = 4, μ = 12.724 mm^{-1}, reflections collected = 30 911, independent reflections = 6344, R_1 = 0.0454, wR_2 = 0.1171 [$F^2 > 2\sigma(F^2)$], R_1 = 0.0503, wR_2 = 0.1200 (all data). Crystal data **6** at 100 K: $C_{58}H_{46}IrO_{13}S_{40}$, M = 2425.56, black prism, a = 18.37840(10), b = 13.17680(10), c = 33.6413(3) Å, β = 94.0750(10)°, U = 8126.27(11) Å^3, T = 100(2) K, space group $C2/c$, Z = 4, μ = 13.310 mm^{-1}, reflections collected = 38 584, independent reflections = 7628, R_1 = 0.0314, wR_2 = 0.0820 [$F^2 > 2\sigma(F^2)$], R_1 = 0.0322, wR_2 = 0.0824 (all data). Crystal data **6** at 150 K: $C_{58}H_{46}IrO_{13}S_{40}$, M = 2425.56, black prism, a = 18.4349(2), b = 13.18390(10), c = 33.6063(2) Å, β = 94.1340(10)°, U = 8146.55(12) Å^3, T = 150.01(10) K, space group $C2/c$, Z = 4, μ = 13.276 mm^{-1}, reflections collected = 15 759, independent reflections = 7803, R_1 = 0.0350, wR_2 = 0.0876 [$F^2 > 2\sigma(F^2)$], R_1 = 0.0383, wR_2 = 0.0899 (all data). Crystal data **6** at 290 K: $C_{56}H_{40}IrO_{12}S_{40}$ + solvent, M = 2379.50, black prism, a = 18.6386(15), b = 13.2500(8), c = 33.689(2) Å, β = 94.474(6)°, U = 8294.5(10) Å^3, T = 290.03(10) K, space group $C2/c$, Z = 4, μ = 13.016 mm^{-1}, reflections collected = 7329, independent reflections = 5332, R_1 = 0.0964, wR_2 = 0.2453 [$F^2 > 2\sigma(F^2)$], R_1 = 0.1199, wR_2 = 0.2645 (all data).

4 : 1 Pseudo-κ salt with tris(oxalato)iridate

Pseudo-κ-(BEDT-TTF)$_4$[$(H_3O)Ir(C_2O_4)_3$]·PhCN (5). The first members of the BEDT-TTF-tris(oxalato)metallate family, (BEDT-TTF)$_4$[(A)Fe$(C_2O_4)_3$]·PhCN,[3] were a superconducting β″ salt (A = H_3O^+) and a semiconducting pseudo-κ polymorph (A = K^+ and NH_4^+). Both β″ and pseudo-κ phases have also been obtained when using tris(oxalato)chromate instead of -ferrate (A = H_3O^+ in both phases). The superconducting T_cs of these β″ salts with benzonitrile are some of the highest in the family so there has been interest in obtaining β″ salts with other tris(oxalato)metallates. However, when the tris(oxalato)metallate is aluminate, cobaltate, manganate, rhodate or ruthenate, only the semiconducting pseudo-κ phase has been obtained regardless of whether A = H_3O^+, K^+ or NH_4^+.

A large number of guest molecules have been included in this family of salts but the pseudo-κ phase is only obtained when the guest is benzonitrile (or a mixture of benzonitrile with a 2nd guest – nitrobenzene or dichlorobenzene).

Here we report the results of crystal growth of BEDT-TTF with tris(oxalato)iridate with benzonitrile as a guest which gives only the semiconducting pseudo-κ phase (BEDT-TTF)$_4$[$(H_3O)Ir(C_2O_4)_3$]·PhCN and no crystals of β″. The best crystals were obtained when using the crystal growth method which includes 1,2,4-trichlorobenzene.[25] Using the method of Peter Day's group that was used to prepare the β″ Fe[3] and Cr[10] phases in the original salts also gave only pseudo-κ crystals with Ir.

The structure of pseudo-κ-(BEDT-TTF)$_4$[$(H_3O)Ir(C_2O_4)_3$]·PhCN (**5**) is isostructural with the previously reported salts in

Open Access Article. Published on 13 May 2022. Downloaded on 10/20/2025 10:18:24 PM.
This article is licensed under a Creative Commons Attribution-NonCommercial 3.0 Unported Licence.

Table 4 X-Ray data for salts **1–4**‡

	Ga-PhF (**1**)	Ga-PhCl (**2**)	Ga-PhBr (**3**)	Ga-PhI (**4**)
Formula	$C_{52}H_{40}FO_{13}GaS_{32}$	$C_{52}H_{40}ClO_{13}GaS_{32}$	$C_{52}H_{40}BrO_{13}GaS_{32}$	$C_{52}H_{40}IO_{13}GaS_{32}$
Fw [g mol^{-1}]	1987.52	2003.93	2048.39	2095.38
Crystal system	Monoclinic	Monoclinic	Monoclinic	Monoclinic
Space group	*C*2/*c*	*C*2/*c*	*C*2/*c*	*C*2/*c*
Z	4	4	4	4
T (K)	294(2)	293(2)	293(2)	294(2)
a [Å]	10.2801(4)	10.2964(7)	10.2880(3)	10.2593(2)
b [Å]	19.8975(10)	19.9923(14)	19.9599(6)	20.0074(4)
c [Å]	35.2455(13)	35.423(3)	35.5191(8)	35.5849(7)
α [°]	90	90	90	90
β [°]	92.680(3)	93.080(3)	93.392(2)	93.7398(18)
γ [°]	90	90	90	90
Volume [Å^3]	7201.5(5)	7281.3(9)	7280.98(16)	7288.67(14)
Density [g cm^{-3}]	1.832	1.828	1.871	1.911
μ [mm^{-1}]	1.373	1.392	1.905	1.778
R_1	0.0709	0.0745	0.0573	0.0413
w*R* [all data]	0.1479	0.1447	0.1254	0.0934

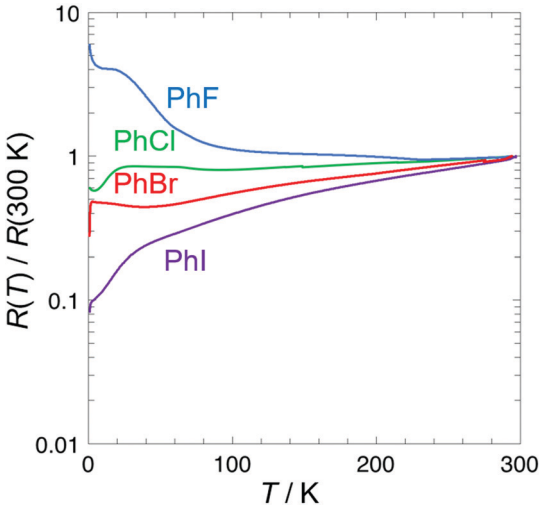

Fig. 6 Electrical resistivity for salts **1–4**.

the family, crystallising in the orthorhombic space group *Pbcn* with two crystallographically independent BEDT-TTF donors, half a tris(oxalato)iridate anion, half a benzonitrile guest molecule, and half an H_3O^+ counter cation.

Fig. 7 shows the alternating donor and anion layers. Fig. 8 shows the pseudo-κ packing motif of the BEDT-TTFs in the donor layer. Short S···S contacts are given in Table 5. (BEDT-TTF$^+$)$_2$ dimers are surrounded by six BEDT-TTF^0 monomers which are responsible for the semiconducting behaviour observed in these salts (Table 6).

The anion layer (Fig. 9) is a honeycomb arrangement of $Ir(C_2O_4)_3^{3-}$ and H_3O^+. The benzonitrile molecule sits in the honeycomb's hexagonal cavity with the nitrile group disordered over two positions pointing towards H_3O^+ cations (Fig. 10 and Table 3). The hexagonal cavity is therefore wider than in the β″ phase (Fig. 4 and Table 3). Every anion layer in the pseudo-κ phase is built up of alternating rows of the Δ and Λ enantiomers of the tris(oxalato)iridate. The β″ phase differs in the dispersion of enantiomers in having an entire anion layer consisting of a single enantiomer whilst the adjacent anion layers consist of the opposite enantiomer. Both result in a net overall racemic lattice.[3,10]

Previously reported pseudo-κ-(BEDT-TTF)$_4$[(A)M^{3+}(C$_2$O$_4$)$_3$]·PhCN salts are all semiconductors with an E_a between

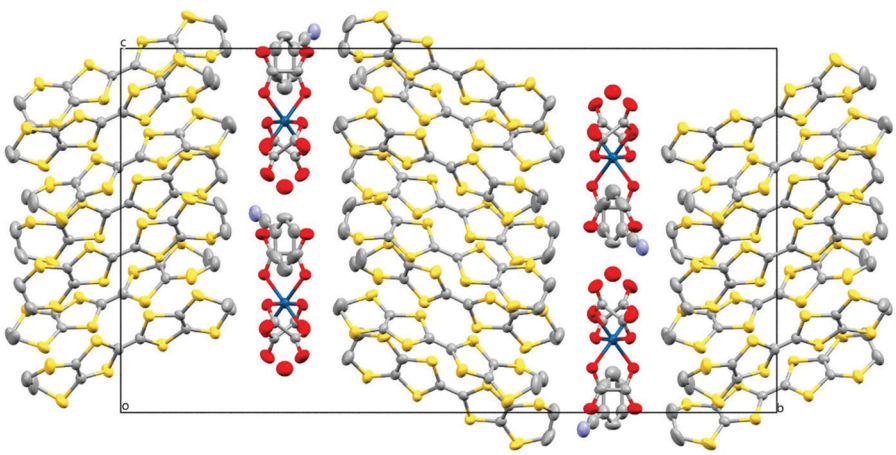

Fig. 7 Structure of **5** viewed down the *a* axis. Hydrogen atoms and minor disorder components are omitted for clarity.

 © 2022 The Author(s). Published by the Royal Society of Chemistry

Open Access Article. Published on 13 May 2022. Downloaded on 10/20/2025 10:18:24 PM.
This article is licensed under a Creative Commons Attribution-NonCommercial 3.0 Unported Licence.

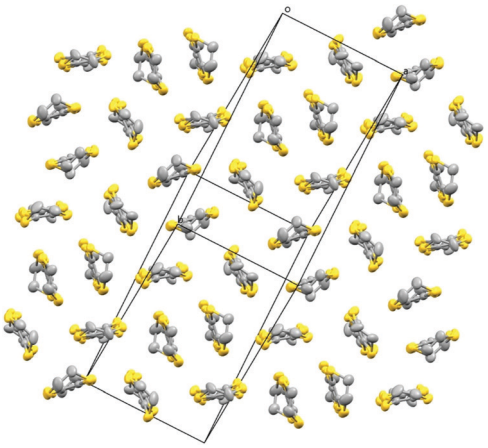

Fig. 8 Packing arrangement of the donor layer for **5**. Hydrogen atoms and minor disorder components are omitted for clarity.

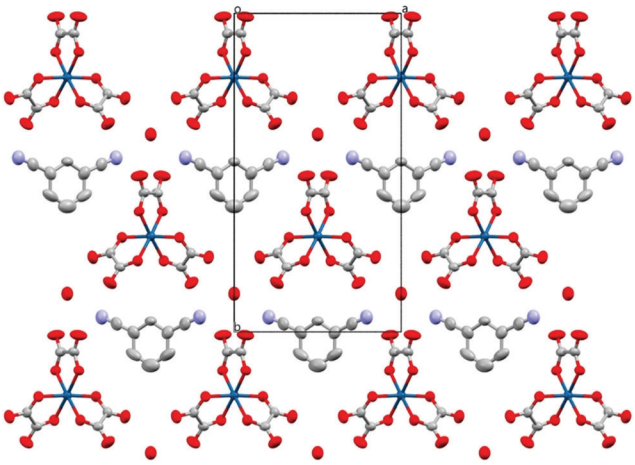

Fig. 9 Packing arrangement of the anion layer for **5** viewed down the *c* axis. Hydrogen atoms and minor disorder components are omitted for clarity.

Table 5 Short range interactions (>sum VdW radii) for donor cations in salt **5**

Contact (Å)	Ir-PhCN (**5**)
S1···S14	3.2190(17)
S1···S16	3.4418(19)
S7···S10	3.4384(18)
S2···S15	3.5170(19)
S8···S9	3.5214(18)
S2···S11	3.4333(17)
S6···S15	3.5106(18)
S11···S14	3.4460(17)
S12···S13	3.4768(17)

Table 6 Average bond lengths (Å) in BEDT-TTF molecules in salt **5** with approximation of the charge on the molecules. $\delta = (b + c) - (a + d)$, $Q = 6.347-7.463\delta$[21]

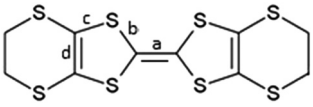

Salt **5**	Donor	*a*	*b*	*c*	*d*	δ	*Q*
	A	1.381	1.725	1.743	1.3505	0.736	+0.85
	B	1.343	1.756	1.758	1.340	0.831	+0.15

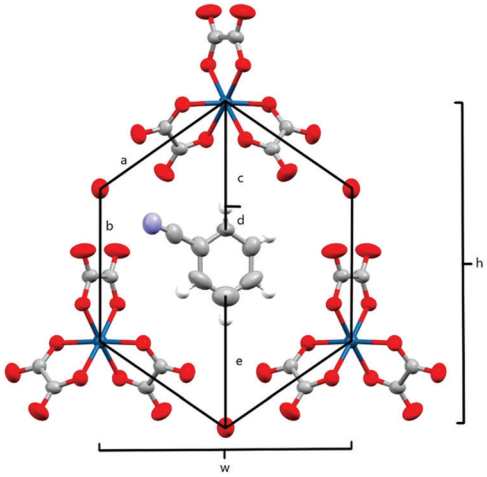

Fig. 10 Honeycomb cavity in the anion layer for **5** with measurement parameters labelled.

140 and 245 meV.[8] Salt **5** also shows semiconducting behaviour (Fig. 11) with an E_a of 116 meV.

5 : 1 salt with tris(oxalato)iridate

β″-(BEDT-TTF)$_5$Ir(C$_2$O$_4$)$_3$·EtOH (6). We recently published a 2 : 1 salt, β″-(BEDT-TTF)$_2$[(H$_2$O)(NH$_4$)$_2$Ir(C$_2$O$_4$)$_3$]·18-crown-6, which was the first example in this family to contain a 5d tris(oxalato)metallate anion.[18] A 4 : 1 BEDT-TTF salt has previously been reported with 5d bis(oxalato)platinate, Pt(C$_2$O$_4$)$_2^{2-}$, which shows metallic behaviour down to 60 K.[26]

When using benzonitrile with tris(oxalato)iridate in salt **5** we have also used halobenzenes with tris(oxalato)iridate but no crystals could be obtained, in contrast to the relative ease with which they can be obtained when using the 3d and 4d tris(oxalato)metallates.

Crystals of a 5 : 1 salt (**6**) have been obtained using acetophenone as the electrocrystallisation solvent with either the ammonium or potassium salt of tris(oxalato)iridate (Fig. 12). Two 5 : 1 salts in the BEDT-TTF-tris(oxalato)metallate family have previously been reported and both are semiconductors. Instead of the hexagonal anion layer packing arrangement found in the 2 : 1,[18] 3 : 1,[17] and 4 : 1[3,8] salts the tris(oxalato)ferrate anions are arranged in a parallelogram. (BEDT-TTF)$_5$[Fe(C$_2$O$_4$)$_3$]·(H$_2$O)$_2$·CH$_2$Cl$_2$[27] has an anion layer containing only a single enantiomer of tris(oxalato)ferrate with the adjacent anion layers being the opposite enantiomer. The

Open Access Article. Published on 13 May 2022. Downloaded on 10/20/2025 10:18:24 PM.
This article is licensed under a Creative Commons Attribution-NonCommercial 3.0 Unported Licence.

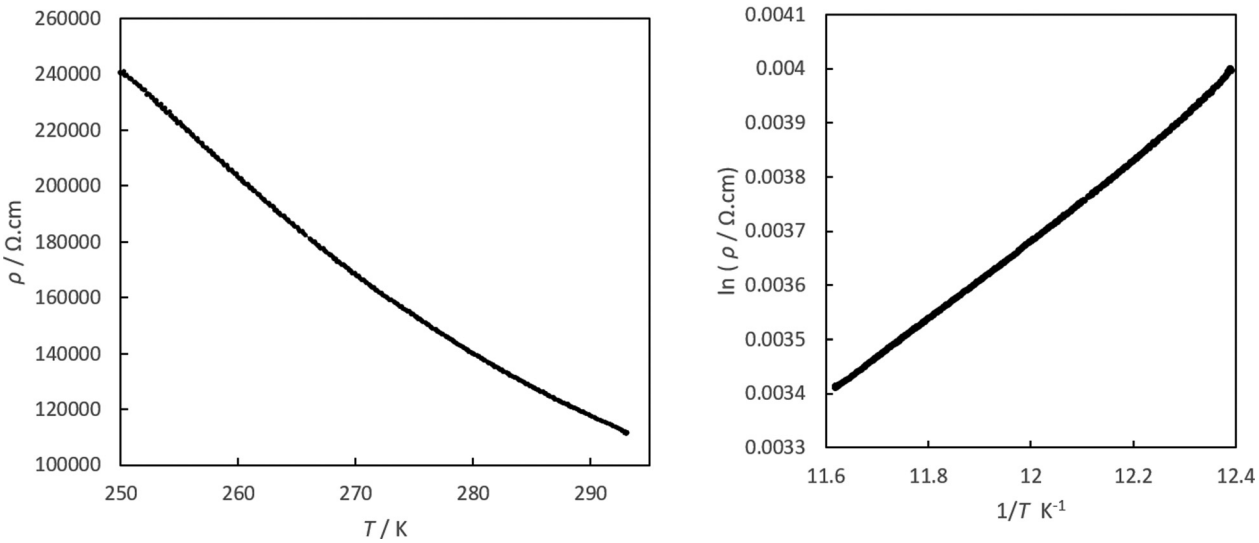

Fig. 11 Electrical resistivity for salt **5**.

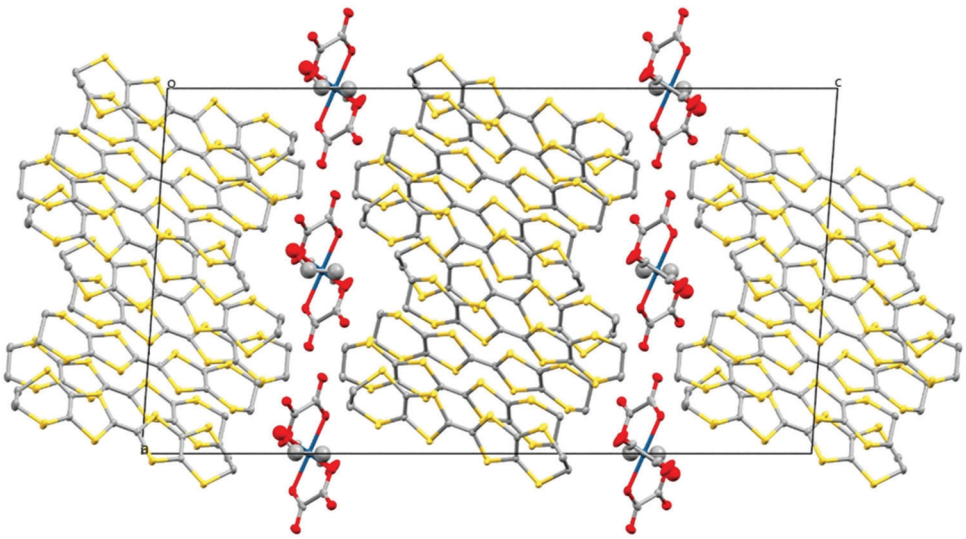

Fig. 12 Structure of **6** viewed down the *b* axis. Hydrogen atoms and minor disorder components are omitted for clarity.

parallelogram contains a CH_2Cl_2 and two H_2O molecules. α″-(BEDT-TTF)$_5$[Ga(C_2O_4)$_3$]·(H_2O)$_{3.4}$·(EtOH)$_{0.6}$[23] differs with every anion layer containing a 50 : 50 mixture of each tris(oxalate)gallate enantiomer and a parallelogram containing disordered ethanol and water molecules in a void on one side.

Salt (**6**) differs from these previously reported 5 : 1 salts in having a β″ donor packing arrangement (Fig. 13) with a diamond-shaped packing of tris(oxalato)iridate in the anion layers with no included water molecules (Fig. 14). Salt **6** crystallises in the monoclinic space group *C*2/*c*, with two and a half crystallographically independent BEDT-TTF molecules, half an Ir(C_2O_4)$_3^{3-}$ anion, and a disordered ethanol molecule. The crystal structure is built up of alternating layers of BEDT-TTF in a β″ packing motif and layers of Ir(C_2O_4)$_3^{3-}$/ethanol (Fig. 12).

Each anion layer contains only a single enantiomer of Ir(C_2O_4)$_3^{3-}$, with the adjacent anion layers containing only the opposite enantiomer to give an overall racemic lattice (Fig. 14). The tris(oxalato)iridate anions adopt a diamond shaped arrangement with 11.332 Å between every iridium atom, and a disordered ethanol molecule within the cavity between anions.

The two and half crystallographically independent BEDT-TTF molecules, where A, B and C are coloured yellow, blue and red, respectively, in Fig. 13 and 16, follow an –AABCBAABCB– pattern within each stack. There are a number of side-to-side S···S interactions between donor stacks which are below the sum of the van der Waals radii (Table 7) but there are none face-to-face within a stack. The BEDT-TTF donor molecules denoted

 © 2022 The Author(s). Published by the Royal Society of Chemistry

Open Access Article. Published on 13 May 2022. Downloaded on 10/20/2025 10:18:24 PM.
This article is licensed under a Creative Commons Attribution-NonCommercial 3.0 Unported Licence.

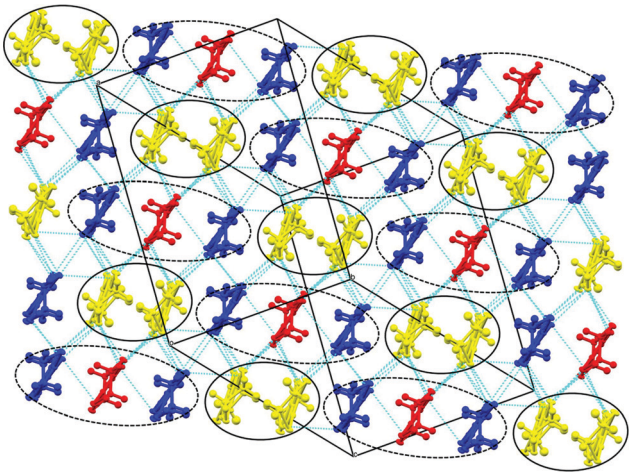

Fig. 13 Packing arrangement of the donor layer for **6**. Donor A = yellow, B = blue, C = red.

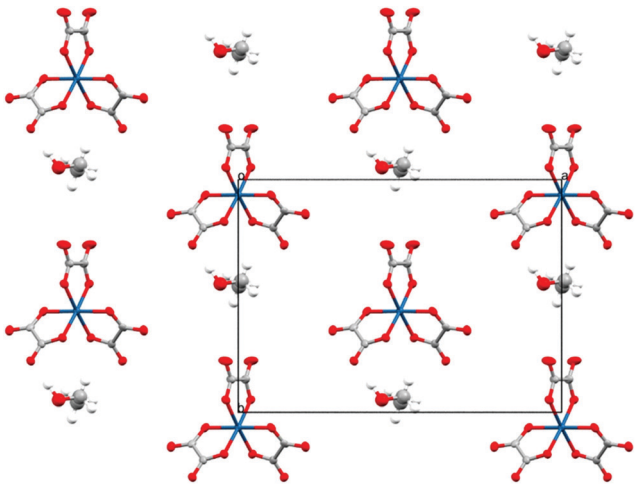

Fig. 14 Packing arrangement of the anion layer for **6** viewed down the *c* axis.

Table 7 Short range interactions (>sum VdW radii) for donor cations in salt **6** in Å

Contact (Å)	Ir-EtOH (**6**) 100 K	Ir-EtOH (**6**) 150 K	Ir-EtOH (**6**) 298 K
S1···S3[a]	3.4725(11)	3.4745(11)	3.521(6)
S1···S11[a]	3.4159(12)	3.4273(11)	3.469(5)
S1···S12[a]	3.4122(11)	3.4285(11)	3.490(5)
S3···S9[a]	3.5057(11)	3.5167(11)	3.558(5)
S4···S9[a]	3.5775(11)	3.5893(11)	3.634(5)
S5···S16[b]	3.5337(13)	3.5400(12)	3.607(7)
S6···S8[b]	3.5810(11)	3.5854(11)	3.615(5)
S6···S16[b]	3.4319(12)	3.4442(12)	3.526(6)
S8···S13[b]	3.5046(10)	3.5138(10)	3.560(6)
S9···S17[c]	3.3585(10)	3.3701(10)	3.417(5)
S9···S18[c]	3.4240(12)	3.4356(12)	3.495(5)
S13···S18	3.5533(12)	3.5661(11)	3.581(5)
S14···S18	3.3542(11)	3.3648(11)	3.413(5)
S16···S19[d]	3.3860(11)	3.4022(11)	3.457(5)
S16···S20[d]	3.3683(11)	3.3792(11)	3.431(5)

[a] $1-x, -y, 1-z$. [b] $1.5-x, 0.5-y, 1-z$. [c] $1-x, 1-y, 1-z$. [d] $1.5-x, 1.5-y, 1-z$.

A (Fig. 13, 15 and 16) form a dimer which is twisted by only 2.6° with respect to the trimer formed using donors B and C. In Fig. 13, we show solid line ellipsoids on the A–A dimers and dashed line ellipsoids on the B–C–B trimers. As mentioned in Fig. 15a, the intermolecular interactions for A–A dimers and B–C–B trimers are relatively strong and weak, respectively. Using the method of Guionneau *et al.*[21] to estimate the charge on a BEDT-TTF molecule from its C–S and C═C bond lengths we estimate a charge on each donor (Table 8). This gives the expected 3+ overall charge for five donors balancing the charge of the anion $[Ir(C_2O_4)_3]^{3-}$. Salt **6** is metallic down to 50 K below which there is a transition to insulating behaviour for the cooling process (Fig. 17). The metal–insulator transition temperature in the heating process is the same as that of the cooling process, but a weak-semiconducting or semi-metallic behaviour is observed from 50 to 225 K. Above 225 K metallic behaviour is observed up to room temperature. Band calculations are performed at 100, 150 and 290 K. The results are shown in Fig. 15. The Fermi surfaces at 290 and 150 K (Fig. 15e and d) are simply cylindrical, suggesting that at each temperature the salt is a stable 2D metal. However, Table 8 suggests a tendency for charge disproportionation. Normalized charges (Q_n) suggest that donor A is almost monocationic and C is almost neutral. Therefore, the A–A dimer is dicationic, meaning that spin dimers are formed and hence the dimers do not play any role in the electrical conductivity. C is neutral, meaning that the valence orbital is fully occupied, suggesting that C also has no conducting carriers. The valence orbitals of only B are partially occupied and interact with each other along the $a + b$ direction (≈//side-by-side direction). Actually, the Fermi surface in Fig. 15d has a wide flat region along the a'*-axis in the primitive lattice (≈//side-by-side direction), indicating that this direction is the most conductive. In contrast, at 150 K the A–A dimer and C molecule become monocationic as an electron moves from the A–A dimer to C. At this temperature the cooling curve has no anomaly but the heating curve has an anomaly at 225 K, where the phase transition appears to occur. The resultant B–C–B trimer is dicationic therefore there is a spin dimer on each trimer. Therefore, only the partially occupied monocationic A–A dimer is conductive. However, as shown in Fig. 13, the A–A dimers are isolated by the dicationic B–C–B trimers, suggesting that the charge disproportionate state at 150 K seems to be less conductive than that at 290 K, which was realized on the heating resistivity curve. Although the charge disproportionate states were realized at both temperatures, the salt shows low resistivity in this temperature range. A conductive charge-ordered state is also observed in θ-(BEDT-TTF)$_2$CsCo(NCS)$_4$.[28] In addition, there is an incorporated EtOH molecule in the unit cell. It is heavily disordered at 290 K and ordered over two positions at 150 K. The incorporated EtOH molecule is located close to the C BEDT-TTF molecule. So, we guess that the dipole moment of the ordered EtOH may play a significant role in changing the charge of C from neutral at 290 K to cationic at 150 K. As mentioned above, the Fermi surfaces at 290 and 150 K are cylindrical, which suggests that both are stable metals. However, each band dispersion has a

Open Access Article. Published on 13 May 2022. Downloaded on 10/20/2025 10:18:24 PM.
This article is licensed under a Creative Commons Attribution-NonCommercial 3.0 Unported Licence.

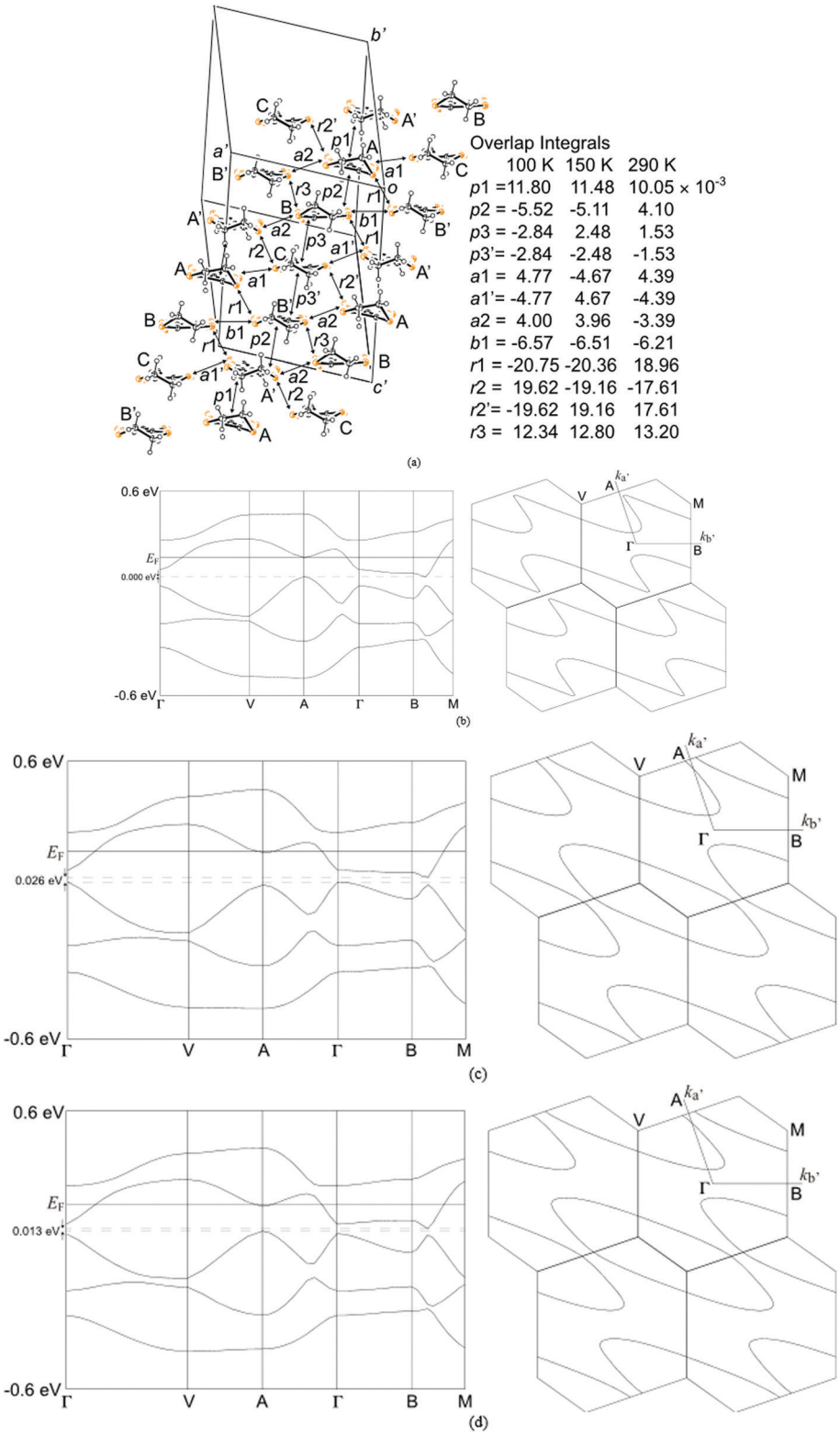

Fig. 15 (a) Donor arrangement at 100 K and overlap integrals, band dispersions and Fermi surfaces of salt **6** at 100 (b), 150 (c) and 290 K (d)*[1]. *[1] Because of the software's restriction*[1] the band calculation was performed after a unit cell transformation from the *C*-centered lattice (*x*, *y*, *z*) to a primitive lattice (x', y', z') = ($-0.5x - 0.5y$, $-0.5x + 0.5y$, $-z$). The resulting cell parameters are as follows; a' = 11.307, 11.332 and 11.434, b' = 11.307, 11.332 and 11.434, c' = 33.641, 33.606 and 33.698 Å, α' = 93.31, 93.36 and 93.65, β' = 93.31, 93.36 and 93.65, γ' = 71.28, 71.14 and 70.82°, for 100, 150 and 290 K, respectively, where a^* is parallel to the side-by-side direction and b^* is close to and parallel to the stacking direction. *[1] T. Mori, A. Kobayashi, Y. Sasaki, H. Kobayashi, G. Saito and H. Inokuchi, *Bull. Chem. Soc. Jpn.*, 1984, **57**, 627–633.

 © 2022 The Author(s). Published by the Royal Society of Chemistry

Open Access Article. Published on 13 May 2022. Downloaded on 10/20/2025 10:18:24 PM.
This article is licensed under a Creative Commons Attribution-NonCommercial 3.0 Unported Licence.

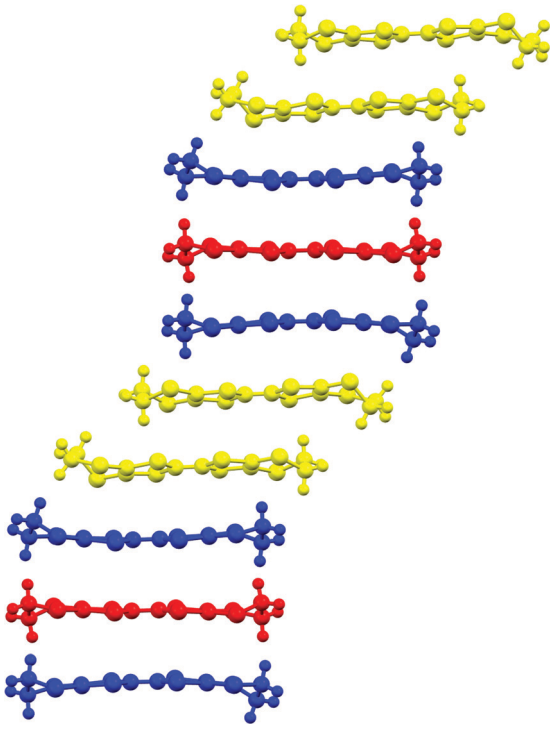

Fig. 16 Packing arrangement of the donor layer for **6**. A = yellow, B = blue, C = red.

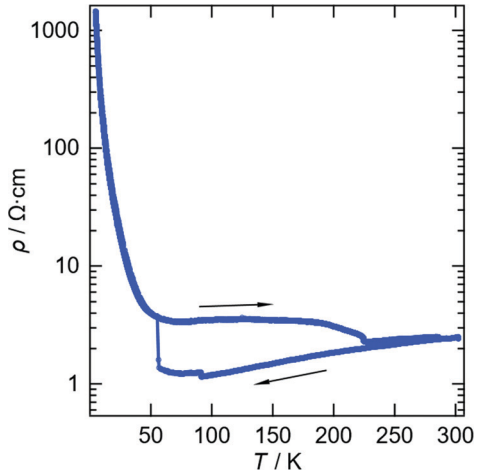

Fig. 17 Electrical resistivity for salt **6**.

gap between the third and fourth lines from the bottom and the gap at 150 K is wider than that at 290 K. We do not know the exact effect of the gap but usually such a gap causes localization of electrons. In addition, the charge of C of 0.79 at 150 K is not so close to 1.0. We suggest that the value is close to 1.0 just below the transition temperature because Table 8 indicates no charge disproportionation at 100 K, namely the charges of A, B and C are ≈ 0.6 which is equal to the BEDT-TTF formula charge of **6**. The lower the temperature the weaker the charge disproportionation, which is somewhat strange, but it was recently reported in a salt.[29] This suggests that the salt at 100 K is more conductive than that at 150 or 290 K. The band dispersions at 100 K have no gap as shown in Fig. 15d, which again suggests no localization. The Fermi surface at 100 K opens along the b'^*-axis (≈//stacking direction). This indicates that the salt is quasi 1D-like below 100 K. These results suggest that a phase transition or crossover occurs between 100 and 150 K. Fig. 17 indicates no anomaly on the cooling curve in this temperature range but a broad peak around 130 K on the heating curve. This might be the temperature at which the phase transition or crossover occurs. We have no structural information below the MI transition. But the discussion above suggests that the salt is not in any charge-ordered states at low temperature. Therefore, a charge-density wave along the side-by-side direction is the most suitable explanation, although it is only speculation.

Conclusions

We report six new additions to the family of salts of BEDT-TTF with tris(oxalato)metallate anions. Four new tris(oxalato)gallate salts are 4 : 1 salts β″-(BEDT-TTF)$_4$[(H$_3$O)Ga(C$_2$O$_4$)$_3$]·halobenzene with fluorobenzene or chlorobenzene as a guest molecule

Table 8 Average bond lengths (Å) in BEDT-TTF molecules for **6** with approximation of the charge on the molecules. $\delta = (b + c) - (a + d)$, $Q = 6.347 - 7.463\delta$[21]

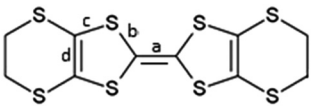

Salt **6**	Donor	a	b	c	D	δ	Q	Q_n[a]		Q_m[b]
100 K	A	1.375	1.736	1.750	1.352	0.759	+0.68	+0.60	A–A dimer	+1.20
	B	1.371	1.737	1.750	1.353	0.763	+0.65	+0.58	B–C–B trimer	+1.81
	C	1.376	1.734	1.753	1.358	0.753	+0.73	+0.65		
150 K	A	1.362	1.737	1.751	1.347	0.779	+0.53	+0.57	A–A dimer	+1.14
	B	1.360	1.738	1.750	1.343	0.785	+0.49	+0.53	B–C–B trimer	+1.85
	C	1.375	1.732	1.752	1.357	0.752	+0.73	+0.79		
290 K	A	1.374	1.730	1.756	1.324	0.788	+0.47	+0.90	A–A dimer	+1.80
	B	1.347	1.735	1.747	1.323	0.812	+0.29	+0.55	B–C–B trimer	+1.20
	C	1.312	1.747	1.751	1.329	0.857	+0.05	+0.10		

[a] Normalised by the total charge. [b] Normalised charges of dimers and trimers.

Open Access Article. Published on 13 May 2022. Downloaded on 10/20/2025 10:18:24 PM.
This article is licensed under a Creative Commons Attribution-NonCommercial 3.0 Unported Licence.

giving metallic behaviour, whilst the larger bromobenzene or iodobenzene shows superconductivity. Two new tris(oxalato)-iridate salts are a semiconducting 4 : 1 salt pseudo-κ-(BEDT-TTF)$_4$[(H$_3$O)Ir(C$_2$O$_4$)$_3$]·benzonitrile and a 5 : 1 metal–insulator β″-(BEDT-TTF)$_5$Ir(C$_2$O$_4$)$_3$·ethanol.

Experimental

Starting materials

Fluorobenzene, chlorobenzene, bromobenzene, iodobenzene, 1,2,4-trichlorobenzene, ethanol and 18-crown-6 were purchased from Sigma-Aldrich and used as received. BEDT-TTF was purchased from TCI and recrystallised from chloroform. Ammonium tris(oxalato)iridate,[30] potassium tris(oxalato)iridate,[30] and ammonium tris(oxalato)gallate[31] were prepared by literature methods and recrystallised several times from water.

Synthesis of radical-cation salts

Radical-cation salts **1–6** were synthesized by dissolving 100 mg of ammonium tris(oxalato)gallate or -iridate with 250 mg 18-crown-6 ether in 10 mL 1,2,4-trichlorobenzene: 2 mL ethanol with 10 mL fluorobenzene (**1**), chlorobenzene (**2**), bromobenzene (**3**), iodobenzene, (**4**), benzonitrile (**5**), or acetophenone (**6**). This was added to a H-shaped electrochemical cell containing 10 mg BEDT-TTF in the anode compartment and a current of 1.0 μA was used for up to a month to obtain a black block (β″ **1–4**), black diamonds (pseudo-κ **5**), or black prisms (**6**).

Electrical resistivity measurements

Temperature dependent electrical resistivity measurements were performed using four contacts on the single crystals of **1–4** along the out-of-plane direction in the range of 0.8–300 K. Measurements were performed using two contacts on the single crystals of **5** in the range of 240–300 K. Measurements were performed using four contacts on the single crystals of **6** in the range of 4–300 K.

X-ray crystallography

Data for **1**, **3–5** and for **6** (at 150 K and 290 K) were collected on a Rigaku Oxford Diffraction Xcalibur System equipped with a Sapphire detector.

Data for **2** were collected on a Rigaku AFC12 goniometer equipped with an enhanced sensitivity (HG) Saturn724+ detector mounted at the window of an FR-E+ SuperBright molybdenum rotating anode generator with VHF Varimax optics (70 μm focus).

Data for **6** (at 100 K) were collected on a Rigaku AFC11 quarter chi goniometer equipped with a Rigaku Hypix 6000 detector mounted at the window of a 007 HF copper rotating anode generator with Varimax optics (300 μm focus).

Author contributions

Synthesis, L. M., A. L. M., E. K. R., L. Q., J. O.; X-ray crystallography, T. J. B., H. A., Y. N., S. J. C., J. C.; conductivity measurements and band calculations S. I., H. A., Y. N., J.-I. Y., T. K.; writing—original draft preparation, L. M., T. J. B., H. A.; project administration, L. M.; funding acquisition, L. M; supervision, L. M., T. J. B.

Conflicts of interest

There are no conflicts to declare.

Acknowledgements

L. M. and T. B. would like to thank the Leverhulme Trust for financial support (RPG-2019-242). L. M. and E. K. R. would like to thank NTU for a PhD studentship. We thank EPSRC for funding the National Crystallography Service.

Notes and references

1 A. M. Kini, U. Geiser, H. H. Wang, K. D. Carlson, J. M. Williams, W. K. Kwok, K. G. Vandervoort, J. E. Thompson and D. L. Stupka, *Inorg. Chem.*, 1990, **29**, 2555–2557.
2 H. Taniguchi, M. Miyashita, K. Uchiyama, K. Satoh, N. Mori, H. Okamoto, K. Miyagawa, K. Kanoda, M. Hedo and Y. Uwatoko, *J. Phys. Soc. Jpn.*, 2003, **72**, 468–471.
3 A. W. Graham, M. Kurmoo and P. Day, *J. Chem. Soc., Chem. Commun.*, 1995, 2061–2062; M. Kurmoo, A. W. Graham, P. Day, S. J. Coles, M. B. Hursthouse, J. L. Caulfield, J. Singleton, F. L. Pratt and W. Hayes, *J. Am. Chem. Soc.*, 1995, **117**, 12209–12217.
4 B. Zhang, Y. Zhang and D. Zhu, *Chem. Commun.*, 2012, **48**, 197–199.
5 E. Coronado, J. R. Galán-Mascarós, C. J. Gómez-García and V. Laukhin, *Nature*, 2000, **408**, 447–449; A. Alberola, E. Coronado, J. R. Galán-Mascarós, C. Giménez-Saiz and C. J. Gómez-García, *J. Am. Chem. Soc.*, 2003, **125**, 10774–10775.
6 A. Akutsu-Sato, H. Akutsu, S. S. Turner, P. Day, M. R. Probert, J. A. K. Howard, T. Akutagawa, S. Takeda, T. Nakamura and T. Mori, *Angew. Chem., Int. Ed.*, 2005, **44**, 291–295.
7 L. Martin, P. Day, H. Akutsu, J. Yamada, S. Nakatsuji, W. Clegg, R. W. Harrington, P. N. Horton, M. B. Hursthouse, P. McMillan and S. Firth, *CrystEngComm*, 2007, **9**, 865–867.
8 S. Benmansour and C. J. Gómez-García, *Magnetochemistry*, 2021, **7**, 93; L. Martin, *Coord. Chem. Rev.*, 2018, **376**, 277–291.
9 T. J. Blundell, M. Brannan, J. Mburu-Newman, H. Akutsu, Y. Nakazawa, S. Imajo and L. Martin, *Magnetochemistry*, 2021, **7**, 90; L. Martin, S. S. Turner, P. Day, P. Guionneau, J. K. Howard, D. E. Hibbs, M. E. Light, M. B. Hursthouse, M. Uruichi and K. Yakushi, *Inorg. Chem.*, 2001, **40**, 1363–1371.
10 L. Martin, S. S. Turner, P. Day, F. E. Mabbs and E. J. L. McInnes, *Chem. Commun.*, 1997, 1367–1368.
11 H. Akutsu, A. Akutsu-Sato, S. S. Turner, D. Le Pevelen, P. Day, V. Laukhin, A. Klehe, J. Singleton, D. A. Tocher, M. R. Probert and J. A. K. Howard, *J. Am. Chem. Soc.*, 2002,

 © 2022 The Author(s). Published by the Royal Society of Chemistry

Open Access Article. Published on 13 May 2022. Downloaded on 10/20/2025 10:18:24 PM.
This article is licensed under a Creative Commons Attribution-NonCommercial 3.0 Unported Licence.

124, 12430–12431; H. Akutsu, A. Akutsu-Sato, S. S. Turner, P. Day, D. A. Tocher, M. R. Probert, J. A. K. Howard, D. Le Pevelen, A.-K. Klehe, J. Singleton and V. Laukhin, *Synth. Met.*, 2003, **137**, 1239–1240; T. G. Prokhorova, L. I. Buravov, E. B. Yagubskii, L. V. Zorina, S. V. Simonov, R. P. Shibaeva and V. N. Zverev, *Eur. J. Inorg. Chem.*, 2014, 3933–3940.

12 S. Benmansour, Y. Sánchez-Máñez and C. J. Gómez-García, *Magnetochemistry*, 2017, **3**, 7.

13 L. Martin, A. L. Morritt, J. R. Lopez, Y. Nakazawa, H. Akutsu, S. Imajo, Y. Ihara, B. Zhang, Y. Zhang and Y. Guo, *Dalton Trans.*, 2017, **46**, 9542–9548.

14 T. G. Prokhorova, L. V. Zorina, S. V. Simonov, V. N. Zverev, E. Canadell, R. P. Shibaeva and E. B. Yagubskii, *CrystEngComm*, 2013, **15**, 7048–7055.

15 H. Akutsu, A. Akutsu-Sato, S. S. Turner, P. Day, E. Canadell, S. Firth, R. J. H. Clark, J. Yamada and S. Nakatsuji, *Chem. Commun.*, 2004, 18–19.

16 L. V. Zorina, S. S. Khasanov, S. V. Simonov, R. P. Shibaeva, V. N. Zverev, E. Canadell, T. G. Prokhorova and E. B. Yagubskii, *CrystEngComm*, 2011, **13**, 2430–2438.

17 L. Martin, P. Day, P. N. Horton, S. Nakatsuji, J. Yamada and H. Akutsu, *J. Mater. Chem.*, 2010, **20**, 2738–2742; L. Martin, H. Akutsu, P. N. Horton and M. B. Hursthouse, *CrystEngComm*, 2015, **17**, 2783–2790; L. Martin, H. Akutsu, P. N. Horton, M. B. Hursthouse, R. W. Harrington and W. Clegg, *Eur. J. Inorg. Chem.*, 2015, 1865–1870; L. Martin, P. Day, S. Nakatsuji, J. Yamada, H. Akutsu and P. Horton, *CrystEngComm*, 2010, **12**, 1369–1372.

18 A. L. Morritt, J. R. Lopez, T. J. Blundell, E. Canadell, H. Akutsu, Y. Nakazawa, S. Imajo and L. Martin, *Inorg. Chem.*, 2019, **58**, 10656–10664; L. Martin, J. R. Lopez, H. Akutsu, Y. Nakazawa and S. Imajo, *Inorg. Chem.*, 2017, **56**(22), 14045–14052; L. Martin, A. L. Morritt, J. R. Lopez, H. Akutsu, Y. Nakazawa, S. Imajo and Y. Ihara, *Inorg. Chem.*, 2017, **56**(2), 717–720.

19 L. Martin, P. Day, W. Clegg, R. W. Harrington, P. N. Horton, A. Bingham, M. B. Hursthouse, P. McMillan and S. Firth, *J. Mater. Chem.*, 2007, **31**, 3324–3329; L. Martin, P. Day, S. A. Barnett, D. A. Tocher, P. N. Horton and M. B. Hursthouse, *CrystEngComm*, 2008, **10**, 192–196.

20 L. Martin, P. Day, S.-I. Nakatsuji, J.-I. Yamada, H. Akutsu, P. N. Horton and M. B. Hursthouse, *Bull. Chem. Soc. Jpn.*, 2010, **83**(4), 419–423; J. Lopez, H. Akutsu and L. Martin, *Synth. Met.*, 2015, **209**, 188–191; L. Martin, S. S. Turner, P. Day, P. Guionneau, J. A. K. Howard, M. Uruichi and K. Yakushi, *J. Mater. Chem.*, 1999, **9**, 2731–2736.

21 P. Guionneau, C. J. Kepert, G. Bravic, D. Chasseau, M. R. Truter, M. Kurmoo and P. Day, *Synth. Met.*, 1997, **86**, 1973–1974.

22 E. Coronado, S. Curreli, C. Giménez-Saiz and C. J. Gómez-García, *Inorg. Chem.*, 2012, **51**, 1111–1126.

23 T. G. Prokhorova, E. B. Yagubskii, L. V. Zorina, S. V. Simonov, V. N. Zverev, R. P. Shibaeva and L. I. Buravov, *Crystals*, 2018, **8**, 92.

24 S. Imajo, H. Akutsu, A. Akutsu-Sato, A. L. Morritt, L. Martin and Y. Nakazawa, *Phys. Rev. Res.*, 2019, **1**, 033184.

25 T. G. Prokhorova, L. I. Buravov, E. B. Yagubskii, L. V. Zorina, S. S. Khasanov, S. V. Simonov, R. P. Shibaeva, A. V. Korobenko and V. N. Zverev, *CrystEngComm*, 2011, **13**, 537–545.

26 S. Gärtner, I. Heinen and D. Schweitzer, *Synth. Met.*, 1989, **31**, 199–213.

27 B. Zhang, Y. Zhang, F. Liu and Y. Guo, *CrystEngComm*, 2009, **11**, 2523–2528.

28 M. Watanabe, Y. Nogami, K. Oshima, H. Mori and S. Tanaka, *J. Phys. Soc. Jpn.*, 1999, **68**, 2654–2663.

29 H. Akutsu, A. Kohno, S. S. Turner, S. Yamashita and Y. Nakazawa, *Mater. Adv.*, 2020, **1**, 3171–3175.

30 M. Delephine, *Bull. Soc. Chim. Fr.*, 1917, **21**(4), 157; H. G. Kruszyna, I. Bodek, L. K. Libby and R. M. Milburn, *Inorg. Chem.*, 1974, **13**(2), 434–438.

31 N. Bulc, L. Golic and J. Siftar, *Acta Crystallogr.*, 1984, **40**, 1829; P. Neogi and N. K. J. Dutt, *J. Indian Chem. Soc.*, 1938, **15**, 83–85.